Desalination and Water Treatment
www.deswater.com

doi: 10.1080/19443994.2015.1127782

57 (2016) 21957–21967
October

Taylor & Francis
Taylor & Francis Group

Comparison of physicochemical properties of activated carbons derived from biomass wastes by $H_4P_2O_7$ activation: adsorption of trimethoprim

Zizhang Guo[a], Li Xu[a], Cui Liu[b], Fengkai Sun[c], Yan Kang[a], Shuang Liang[a,*]

[a]*Shandong Key Laboratory of Water Pollution Control and Resource Reuse, School of Environmental Science and Engineering, Shandong University, Jinan 250100, China, emails: sduguozizhang@163.com (Z. Guo), 68612497@qq.com (L. Xu), kangyan101@163.com (Y. Kang), Tel. +86 531 88361712; Fax: +86 531 88364513; emails: guozzh@163.com, liangshuang@sdu.edu.cn (S. Liang)*

[b]*Department of Mathematics and Statistics, Texas Tech University, Broadway and Boston, Lubbock, TX 79409-1042, USA, email: 1252502255@qq.com*

[c]*Shandong province environmental engineering Co., Ltd. of SAES, Jinan 250100, China, email: guozzh@126.com*

Received 15 August 2015; Accepted 24 November 2015

ABSTRACT

This work investigated the activated carbons (ACs) derived from three kinds of biomass waste carbon precursors, i.e. *Phragmites australis* (PA), mushroom root (MR), and chicken feather (CF) with $H_4P_2O_7$ activation. The effect of different precursors on porous texture, surface chemistry, and adsorption capacities of the derived ACs were comparatively studied. The pore structure and chemical properties of the ACs were characterized by N_2 desorption/adsorption isotherms, element analysis, FTIR, XPS and Boehm's titration methods. It was found that the surface area and pore volume of AC-PA (S_{BET} = 986.8 m^2/g, V_{tot} = 1.07 cm^3/g) and AC-MR (S_{BET} = 950.1 m^2/g, V_{tot} = 1.02 cm^3/g) were about 1.7 times higher than those of AC-CF (S_{BET} = 471.4 m^2/g, V_{tot} = 0.28 cm^3/g). AC-PA (2.488 mmol/g) possessed more acidic oxygen functionalities than AC-MR (1.736 mmol/g) and AC-CF (1.858 mmol/g), while AC-CF had most basic functional groups. Batch adsorption studies were performed to compare the adsorptive abilities of different ACs for trimethoprim (TMP). It was found that the adsorption affinities of TMP followed an order of AC-PA (244.9 mg/g) > AC-MR (165.6 mg/g) > AC-CF (124.2 mg/g).

Keywords: Biomass wastes; Activated carbon; Physicochemical properties; Trimethoprim adsorption

1. Introduction

Activated carbon (AC) is one of the most widely used materials in water treatment because of its large surface area, abundant surface functional groups, and exceptional adsorption properties [1]. It can be produced from various materials, such as biomass wastes [2–4], coal [5], polyacrylonitrile [6], phenolic resin [7], and petroleum waste [8]. Among them, biomass wastes appear to be more economic due to its steady stream of origin. The common species of biomass were plant, fungus, and animal. The different contents among various biomass species make each of the corresponding produced ACs exhibit unique properties.

*Corresponding author.

Most previous AC studies were focused on certain materials all belonging to one biomass species [9]. Litter information is available regarding the comparative analysis of the AC derived from different types of biomass species. In this work, ACs were produced from three biomass wastes i.e. *Phragmites australis* (PA), Mushroom roots (MR), and Chicken feather (CF), belonging to the three species of biomass waste, i.e. plant, fungus, and animal, respectively. These biomass wastes, good precursors for ACs preparation [10–12], were conventionally treated via landfill disposal or incineration, leading to extra environmental pollution. The use of them for AC production appears to be a promising way, which simultaneously reduces the cost of raw materials for AC production and extra environmental pollution.

Several activating agents have been reported for the chemical activation process: including phosphoric acid [13], zinc chloride [14], and alkaline metal compounds [15]. Among them, phosphoric acid appears to be a mature and common method [16]. During activation treatment with phosphoric acid, the pore is developed through the reactions, such as dehydration and cross-linking between the phosphoric acid and precursors [17]. In process of activation using phosphoric acid, *ortho*-phosphoric acid is dehydrated and condensed partly into pyrophosphoric acid, $H_4P_2O_7$, at 213°C [18]. The activating agent which transformed into $H_4P_2O_7$ possesses even higher acidity than that of H_3PO_4 [19,20]. It is therefore reasonably expected that the direct use of activating agent H4P2O7, relatively new, may produce the AC with better characteristics.

Trimethoprim (TMP), a kind of antibiotic, is often poorly metabolized and absorbed by humans and animals. Therefore, 60% higher of TMP eventually discharged into the environment in its original form. In addition, TMP exhibits strong resistance to activated sludge bacteria, the residues consequently cannot be sufficiently removed in wastewater treatment plants [21]. It was thus chosen as the adsorbate to evaluate the adsorption capacities of the different ACs under various conditions. The interaction mechanisms between AC and TMP were also investigated.

The overall objective of the presented work is to comparatively evaluate the properties and the TMP adsorption capacities of the ACs that were derived from different precursors, corresponding to the three species of biomass wastes (i.e. plant, fungus and animal), with $H_4P_2O_7$ activation.

2. Materials and methods

2.1. Materials

P. australis (PA), MR, and CF were obtained from Jinan city in Shandong Province, China. The biomass precursors were first washed with distilled water to remove surface adhered impurities and then dried at 105°C for 12 h. The dried precursors were crushed and sieved to 40 mesh particle size by standard sieves (Model Φ 200). All chemical reagents were analytically pure. TMP (purity > 99.6%) from Sangon Biotech (Shanghai, China) was used as the adsorbate. The chemical structure of TMP and speciation under different pH conditions is shown in Fig. 1.

2.2. Preparation of ACs

The preparation conditions were determined according to the previous work [19,22], each precursor was impregnated with $H_4P_2O_7$ solution (45 wt.%) at a ratio of 1:0.9 (g $H_4P_2O_7$/g precursors) with stirring. After impregnation for 12 h at room temperature, the samples were heated up at a rate of 10°C/min to desired temperature and maintained at 500°C for 1 h

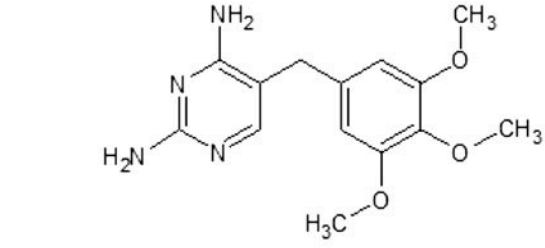

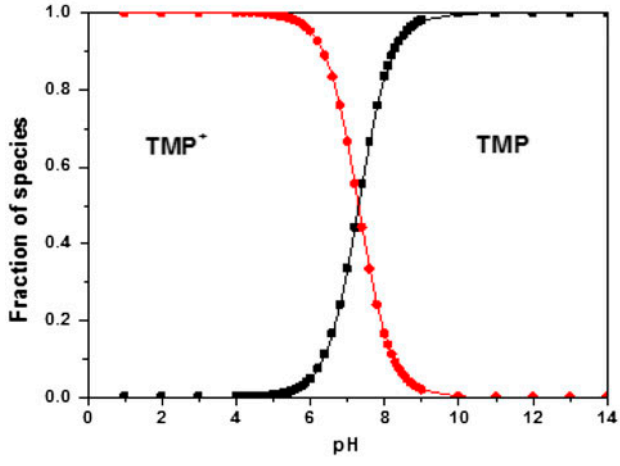

Fig. 1. Chemical structure of TMP and speciation under different pH conditions.

in a muffle furnace in N_2 atmosphere. After activation, the products were washed sequentially with hot water and distilled water to remove redundant impurities until neutral pH of filtrate was obtained. The samples were dried overnight in a vacuum oven at 105°C, and ground and sieved to 140 mesh particle size by standard sieves (Model Φ 200).

2.3. Characterization of ACs

Thermo-gravimetric analysis (TGA) and derivative thermo-gravimetric (DTG) curves of the precursors after $H_4P_2O_7$ impregnation (PA-$H_4P_2O_7$, MR-$H_4P_2O_7$, and CF-$H_4P_2O_7$) were obtained using a TGA (TGA-50 analyzer). The samples were heated from room temperature up to 500°C in nitrogen (100 cm^3/min) atmosphere at a heating rate of 10°C/min.

The BET specific surface area was determined by a multipoint BET method using the adsorption data in the relative pressure (P/P_0) range of 0.05–0.3. Pore size distribution was calculated from the N_2 isotherm at 77 K based on the Density Functional Theory (DFT) method. Micropore surface area (S_{mic}), external surface area (S_{ext}) and micropore volume (V_{mic}) were calculated using the *t*-plot method. Total pore volume (V_{tot}) was determined from the amount of N_2 adsorbed at a P/P_0 around 0.95. Mesopore volume (V_{mes}) was calculated by $V_{tot} - V_{mic}$. Average pore diameter (D_p) was obtained from $D_p = 4V_{tot}/S_{BET}$ by assuming cylindrical pores. For determining the ash contents of the raw materials and ACs, precursors and ACs were ground to pass through 40 mesh particle size by standard sieves (Model Φ 200). One gram of prepared sample was weighed in porcelain basin. Dishes and their contents were placed in muffle furnace at 650°C for 4 h and were then reweighed after they were placed in a desiccator to cool to room temperature [22].

The content of C, H, N, O, and S of ACs was determined using a Vario EI III Element Analyzer (USA). The functional groups available on the surface of ACs were measured using a Fourier transform infrared (FTIR) spectrometer (Fourier-380 FTIR, America) in the spectral range of 4,000–400 cm^{-1}. The surface binding state and elemental speciation of AC was analyzed by X-ray photoelectron spectroscopy (XPS). The measurements were performed by a spectrometer (ESCALAB 250) with Mg Ka irradiation (1,486.71 eV of photons) as X-ray source. All binding energies were referenced to the C 1s peak at 284.6 eV to compensate for the surface charging effects. Boehm's titration method [23] was used to quantify the amount of acidic and basic functional groups on the surfaces of ACs. During the analysis, each sample (0.25 g) was accurately weighed and reacted with 50 mL 0.05 M Na_2CO_3, $NaHCO_3$, NaOH, or HCl in 150 mL conical flasks. Solutions without ACs were used as control. After shaking for 48 h, the remaining alkali or acid was titrated by 0.05 M HCl and 0.05 M NaOH. The different types of functional groups were based on the assumptions that $NaHCO_3$ neutralizes carboxyl groups; Na_2CO_3 neutralizes carboxyl and lactonic groups; NaOH neutralizes carboxyl, lactonic, and phenolic groups; and HCl neutralizes all basic groups.

2.4. Adsorption experiments

Adsorption kinetic experiments were conducted to investigate the effect of agitation time on the adsorption and to determine the kinetic parameters. The experiments were operated as follows: carbon samples (0.2 g) were added to a beaker with 1,000 mL of TMP solutions (0.2 mmol/L); then the mixture was stirred on an electromagnetic stirrer (Model 78–1) at room temperature (25 ± 2°C) and 400 rpm. The samples, withdrawn and filtered at predetermined time intervals (0–36 h), were analyzed to determine the residual concentrations of TMP solution. Batch equilibrium experiments were performed to investigate the effects of initial concentration on the adsorption. A set of 150 mL conical flasks with cover containing 50 mL of TMP solution and 0.01 g of carbons were stirred at 120 rpm in an isothermal water bath shaker for 36 h to ensure that equilibrium was reached at room temperature. Then, the adsorbents were filtered using syringe filter through 0.45 um membrane filters and the residual TMP concentrations were determined with a UV visible spectrophotometer (UV-754, Shanghai) from the absorption at the maximum absorption wavelength of 274 nm. The amount of TMP adsorbed at the equilibrium, Q_e (mg/g), was calculated as Eq. (1):

$$Q_e = (C_0 - C_e)V/W \quad (1)$$

where C_0 and C_e are the initial and equilibrium concentrations of TMP (mg/L), V represents the solution volume (L), and W is the weight of adsorbent (g).

3. Results and discussion

3.1. Thermal analyses of PA-$H_4P_2O_7$, MR-$H_4P_2O_7$, and CF-$H_4P_2O_7$ samples

Fig. 2 shows the TGA and DTG curves for PA-$H_4P_2O_7$, MR-$H_4P_2O_7$, and CF-$H_4P_2O_7$ samples in the temperature range from room temperature to 500°C.

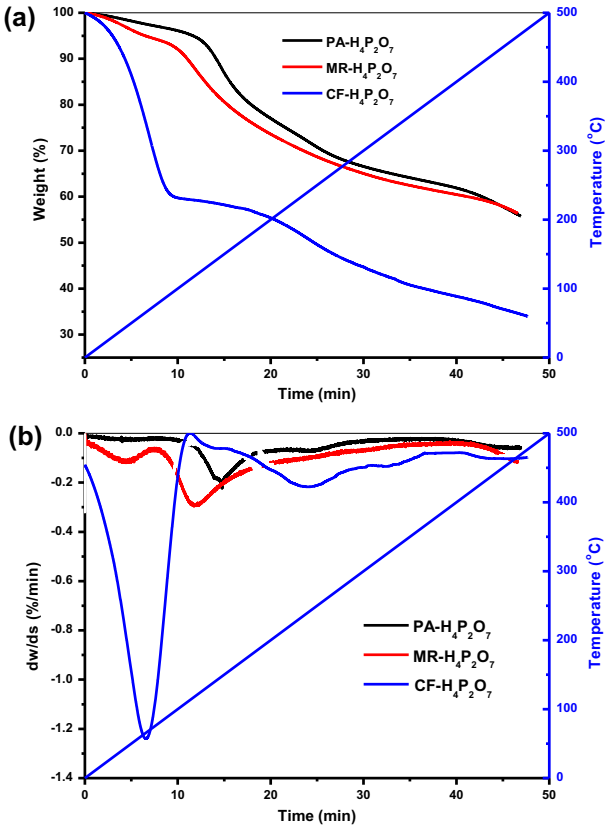

Fig. 2. TGA (a) and DTG (b) curves of PA-$H_4P_2O_7$, MR-$H_4P_2O_7$, and CF-$H_4P_2O_7$ samples.

For the DTG curves, the main peak of PA-$H_4P_2O_7$, MR-$H_4P_2O_7$, and CF-$H_4P_2O_7$ samples appeared successively. This may be because the lignocellulosic precursor has higher pyrolysis temperature. For the TGA curves, the PA- $H_4P_2O_7$ and MR-$H_4P_2O_7$ were higher than CF-$H_4P_2O_7$. This phenomenon may be attributed to the fact that the yields of AC-PA and AC-MR were higher than that of AC-CF, which is further proved by the data of yields listed in Table 1.

3.2. Yields and textural structure of ACs

Pore structure is one of the main physical properties for ACs. The N_2 adsorption/desorption isotherms were conducted to investigate the textural parameters, such as BET surface area, pore volume, and average pore diameter of ACs. It can be seen from Fig. 3 that AC-PA and AC-MR had a wider hysteresis loop at high relative pressures as remarkable characteristic except for AC-CF. Besides, it was found that both AC-PA and AC-MR had mesopores, with D_p of 4.34 nm for AC-PA and 4.29 nm for AC-MR. In contrast, AC-CF exhibited a narrow pore size

Table 1
Sample identification, surface areas, and pore volume parameters for the carbons

Identifications	Yield (%)	S_{BET} (m^2/g)	S_{mic} (m^2/g)	S_{mic}/S_{BET} (%)	S_{ext} (m^2/g)	S_{ext}/S_{BET} (%)	V_{tot} (cm^3/g)	V_{mic} (cm^3/g)	V_{mic}/V_{tot} (%)	V_{mes} (cm^3/g)	V_{mes}/V_{tot} (%)	D_p (nm)
AC-PA	42.1	986.8	234.0	23.7	752.8	76.3	1.07	0.19	17.7	0.88	82.3	4.34
AC-MR	39.7	950.1	289.3	30.4	660.8	69.6	1.02	0.21	20.6	0.71	79.4	4.29
AC-CF	27.5	471.4	312.8	66.4	158.6	33.6	0.28	0.18	63.2	0.10	36.8	2.37

Notes: S_{BET}, BET surface area; S_{mic}, microspore surface area; S_{ext}, external surface area; V_{tot}, total pore volume; V_{mic}, microspore volume; V_{ext}, external volume; D_p, the mean pore diameter.

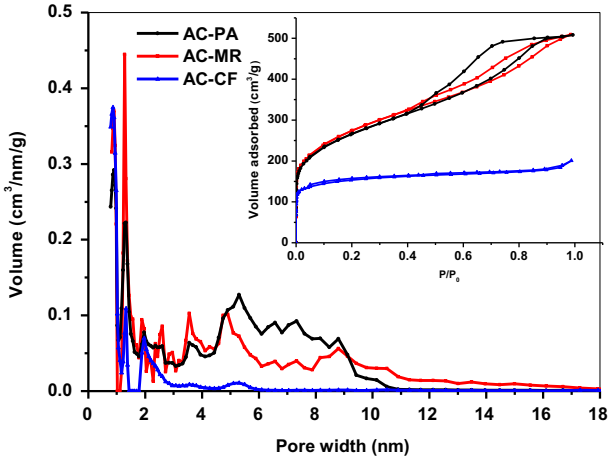

Fig. 3. Pore size distributions and N_2 adsorption/desorption isotherms (inset) for the carbons.

distribution with mainly microporous structures (pore width < 2 nm) with D_p of 2.37 nm. The textural parameters of ACs, included surface area, pore volume, and D_p, prepared from different precursors are calculated and summarized in Table 1. It was noted that the S_{BET} of different ACs followed an order of AC-PA (986.8 m^2/g) > AC-MR (950.1 m^2/g) > AC-CF (471.4 m^2/g). It was also found that AC-PA and AC-MR were highly porous as compared with AC-CF. However, the S_{mic} and V_{mic}/V_{tot} of AC-CF was the highest in all three ACs. It appears that with the microporous structure of ACs increased with the increase in the protein content. In preparation of ACs, lignocellulosic-based precursor could provide more mesoporous structure, and the keratin-based precursor could provide more microporous material.

According to Table 1, AC-PA exhibited higher yields than other ACs. Compared to PA-based and MR-based ACs, CF-based ACs had least yields in three carbons. The reasons might be that $H_4P_2O_7$ promotes the formation of volatiles of biopolymers by bond cleavage reactions during the impregnation stage and keratin materials had more thermosteresis than lignocellulose materials in activation process.

3.3. Chemical characteristics of ACs

Elemental compositions (C, H, O, N, and S) of ACs and their biomass wastes precursors are presented in Table 2. It can be seen that these biomass wastes are very suitable as raw materials for AC preparation because of their high C content (55.4–67.3%) and low ash content (0.5–1.8%). The three types of biomass waste carbon precursors had obvious differences in elemental composition, implying that the AC produced from them may exhibit different surface chemical properties. The contents of C, H, O of PA and MR were very similar, but the content of O of PA and MR was much higher than that of CF. However, the content of N in CF was maximum, followed by MR. Since the MR and CF contained more protein, for the produced ACs, they also presented the same trend and contain more N-containing functional groups. The O/C of AC-PA was the highest because that AC-PA contains most oxygen-containing functional groups in the three carbons. For the produced ACs of CF and MR, they also presented the same trend and contain more N-containing functional groups. After activation of the biomass precursors, the contents of N of AC-MR increased, while that of AC-CF decreased. Especially, the contents of O in AC-MR decreased acutely, but AC-CF changed little. The contents of S in ACs were very low. As the results of the Boehm's titration for the surface functional groups of the carbons are shown in Table 3. It can be seen that the lignocellulose-based ACs have more acidic surface functional groups, while the keratin-based ACs had more basic surface functional groups. It should be noted that the AC-PA (2.488 mmol/g) contains much more acidic surface functional groups, which may enhance its adsorption capacity for TMP. However, the basic surface functional groups of AC-CF (1.450 mmol/g) and AC-MR (1.375 mmol/g) were slightly higher than that of AC-PA (1.262 mmol/g). This may be due to the

Table 2
Elemental composition and ash content of samples before and after the activation

	C (%)	H (%)	O (%)	N (%)	S (%)	O/C (%)	N/C (%)	Ash content (%)
PA	45.1	5.88	48.3	0.47	0.21	107.1	1.04	1.8
MR	42.9	6.50	46.1	3.61	0.89	107.5	8.41	2.0
CF	49.3	7.01	26.2	14.9	2.53	53.1	30.2	0.5
AC-PA	55.4	1.49	41.9	1.01	0.13	75.6	1.82	1.5
AC-MR	67.3	2.09	24.9	5.37	0.36	37.0	7.98	1.1
AC-CF	60.8	2.58	25.5	10.5	0.58	41.9	17.3	0.9

Table 3
Concentrations of surface functional groups of the carbons

Samples	Carboxyl (mmol/g)	Lactone (mmol/g)	Phenolic (mmol/g)	Total acidic (mmol/g)	Basic (mmol/g)
AC-PA	0.724	0.737	1.410	2.488	1.262
AC-MR	0.338	0.576	0.822	1.736	1.375
AC-CF	0.278	0.712	0.869	1.858	1.450

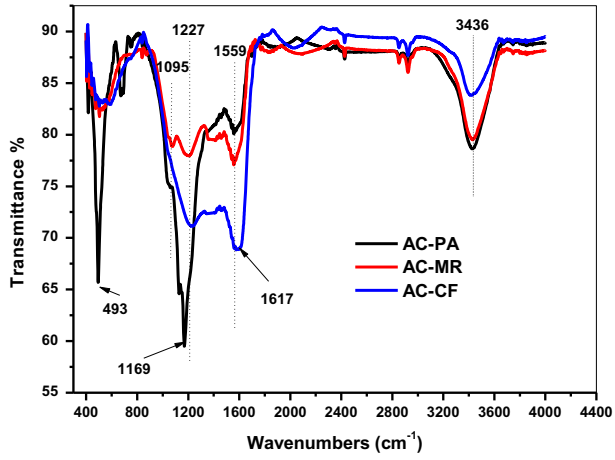

Fig. 4. FTIR spectra of the AC-PA, AC-MR, and AC-CF.

higher content of N in AC-MR and AC-CF than that in AC-PA.

Fig. 4 shows the FTIR spectra of AC-PA, AC-MR, and AC-CF. For all ACs, the bands around 3,436.65 cm^{-1} can be contributed to the O–H stretching vibration or N–H symmetric stretching vibration [24]. The most significant bands were in the regions of 1,559, 1,095, and 493 cm^{-1} for AC-PA and AC-MR, respectively. The peaks at 1,559 cm^{-1} can be attributed to the stretching vibrations of C=O moieties in benzene derivatives [25]. The peaks located around 1,169 and 1,227 cm^{-1} in the FTIR spectra corresponded to the vibrations of C–O in different species, mainly hydroxyl and carboxylic groups [26]. Additionally, AC-PA had the lower transmittance at the band of around 1,169 cm^{-1}, suggesting that AC-PA contains more surface oxygen-containing functional groups. The obtained FTIR spectrum of AC-CF exhibited intensive band at 1,617 cm^{-1}, which is identical to the presence of the amide group [23]. The lower transmittance at the band of around 1,617 cm^{-1} for AC-CF also confirmed that the high N content and more basic functional groups in AC-CF. From Fig. 5, the XPS for the nitrogen-containing functional groups of AC-MR (Fig. 5(a)) and AC-CF (Fig. 5(b)), it was found that there are three peaks at 398.38, 399.43, and 400.40 eV corresponding to the N–H, –CONH–, and CH_2–NH_2 groups, respectively [12].

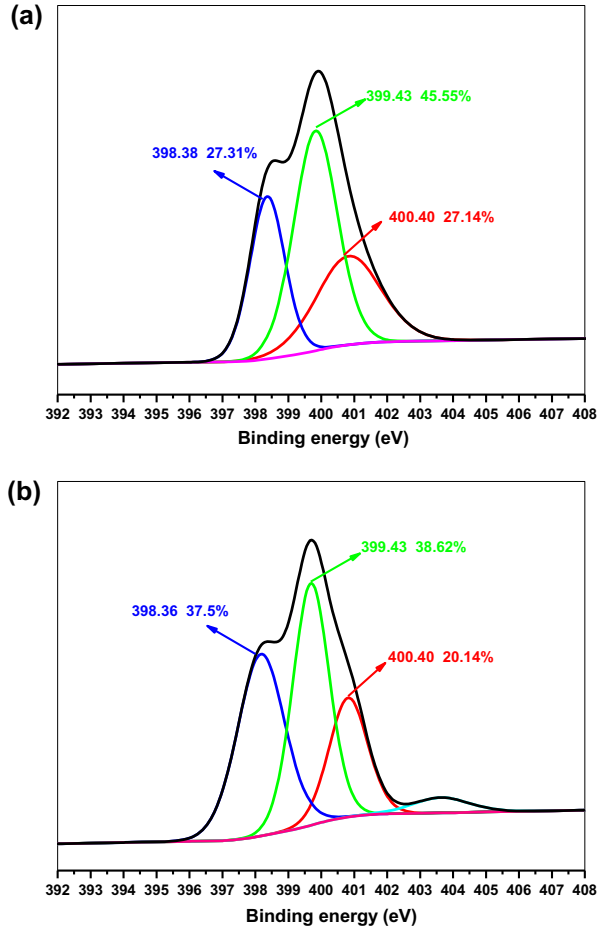

Fig. 5. Curve fitting of the N 1s spectrum of AC-MR (a) and AC-CF (b).

3.4. Comparison of adsorption capacities of TMP

Table 4 shows that AC-PA had larger equilibrium adsorption capacities than AC-MR and AC-CF. AC-PA had an adsorption capacity of 244.9 mg/g, while AC-MR and AC-CF had 165.6 and 124.2 mg/g, respectively. The Q_e of AC-PA (244.9 mg/g) was obviously higher than that of AC-MR (165.6 mg/g), although their S_{BET} were very close. The Q_e of AC-MR (165.6 mg/g) was obviously higher than that of AC-CF (124.2 mg/g), although the acidic functional groups of them were very close. Based on the results

Table 4
Estimated kinetic model constants for TMP adsorption

Kinetic models	Parameter	Activated carbons		
		AC-PA	AC-MR	AC-CF
Pseudo-first-order parameters	$Q_{e,exp}$ (mg/g)	244.9	165.6	124.2
	$Q_{e,cal}$ (mg/g)	95.61	72.09	49.25
	K_1 (1/min)	0.0037	0.0034	0.0035
	R^2	0.9325	0.8971	0.9284
Pseudo-second-order parameters	$Q_{e,exp}$ (mg/g)	244.9	165.6	124.2
	$Q_{e,cal}$ (mg/g)	250.0	166.7	125.0
	K_2 (g mg^{-1} min^{-1} × 10^{-4})	2.216	2.768	4.013
	R^2	0.9999	0.9998	0.9998
Intra-particle diffusion parameters	K_{p1} (mg g^{-1} min$^{-1/2}$)	16.847	7.8092	8.6736
	C_1	56.634	42.776	36.026
	$(R_1)^2$	0.9853	0.9981	0.9924
	K_{p2} (mg g^{-1} min$^{-1/2}$)	3.771	2.0082	1.9378
	C_2	162.54	105.82	78.476
	$(R_2)^2$	0.9683	0.8945	0.9771
	K_{p3} (mg g^{-1} min$^{-1/2}$)	0.4866	0.4345	0.3561
	C_3	226.02	147.28	110.43
	$(R_3)^2$	0.9786	0.9610	0.9585

shown in Tables 1 and 3, the comparison of the S_{BET}, pore structure and surface chemistry characteristic of ACs gave deeper insight into the combined effect of their physical and chemical properties on TMP adsorption. The well-developed pore structure and the rich surface function groups can enhance the adsorption of TMP.

The adsorption mechanisms of TMP inclueded: (1) adsorption and interception function of pore structures, and (2) van der Waals forces, π–π electron-donor-acceptor interactions (π–π EDA), cation-π bonding. The AC-PA and AC-MR had higher porosity than AC-CF. The sorption capacities of AC-PA and AC-MR in terms of TMP were thus larger than that of AC-CF. Also, the TMP molecule contains three methoxy groups (–OCH_3) on its benzene ring. Methoxy group is a strong electron-donating group (see Fig. 1), and consequently makes the benzene ring electron rich. The electron-rich benzene rings can interact strongly with the electron-depleted surfaces of the ACs via π–π EDA interaction. At the test pH of ~6, more than 95% of TMP were protonated. The protonated amino group in the TMP molecule can facilitate strong cation π bonding with π-electrons on the AC surface. It seems reasonable to hypothesize that hydrogen bonding and Lewis acid-base interaction exists between the NH_3^+ groups in TMP and the O-containing groups on AC surface [20].

3.5. Adsorption kinetics

Three commonly used adsorption kinetics (i.e. pseudo-first-order, pseudo-second-order, and intra particle diffusion models) were applied for the experimental data to understand the adsorption mechanism:

$$\ln(Q_e - Q_t) = \ln Q_e - k_1 t \quad (2)$$

$$\frac{t}{Q_t} = \frac{1}{k_2 Q_e^2} + \frac{1}{Q_e} t \quad (3)$$

$$Q_t = k_{pi} t^{1/2} + C_i \quad (4)$$

where Q_e and Q_t (mg/g) are the amount of TMP adsorbed on the adsorbents at equilibrium and at time t, respectively; k_1 (1/min) in Eq. (2) and k_2 (mg min) in Eq. (3) are the pseudo-first-order and pseudo-second-order rate constants. k_{pi} (mg/(g min$^{1/2}$)) in Eq. (4) is the diffusion rate constant of intra-particle, C_i gives an idea about the thickness of boundary layer [27,28].

Information on the kinetics of TMP adsorption is required to select the adapt operation time for batch TMP removal processes. The effect of contact time on TMP adsorbed onto AC-PA, AC-MR, and AC-CF is presented in Fig. 6(a). The adsorption kinetics of TMP was determined for a starting concentration of 58 mg/L (0.2 mmol/L). For ACs, the concentration

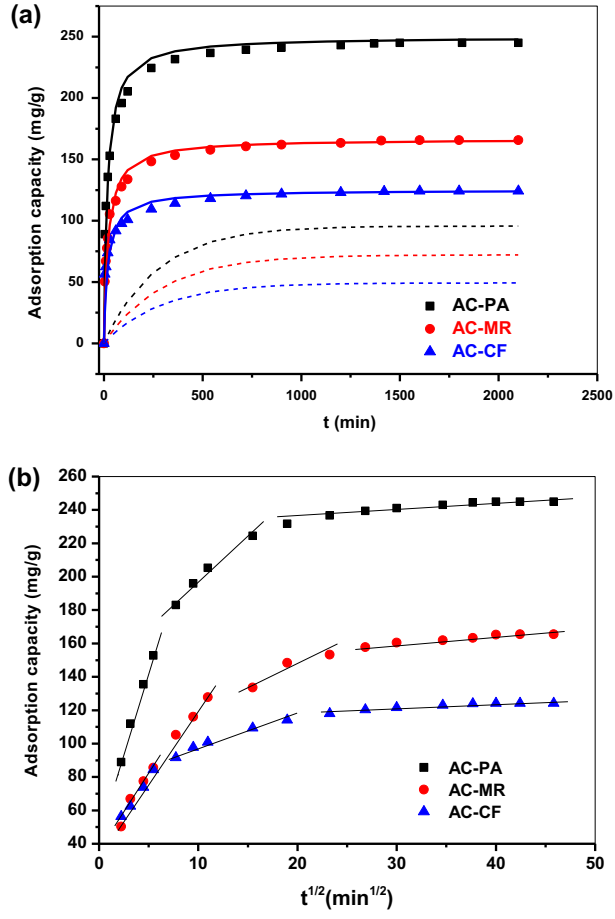

Fig. 6. (a) Adsorption kinetics of TMP on AC-PA, AC-MR, and AC-CF. Dashed lines stand for Pseudo-first-order fit and solid lines stand for Pseudo-second-order fit. (b) Adsorption kinetics using intra-particle diffusion model.

decreased drastically in the first 4 h. Then the equilibrium was gradually achieved within 9 h. In order to ensure sufficient contact time, further adsorption experiments were carried out for 36 h. The calculated kinetic parameters and the correlation coefficient were listed in Table 4. For all ACs, the correlation coefficients of pseudo-second-order kinetics were higher than 0.999. In addition, the calculated Q_e values fitted very well with the experimental data. This tendency indicates that the process in the adsorption of TMP were chemical adsorption involving valence forces through the sharing or exchange of electrons between sorbent and sorbate, complexation, coordination, and/or chelation [20,29]. From Table 4, the highest values of rate constant k_2 were obtained for AC-CF, which demonstrated fastest adsorption kinetics for AC-CF in three ACs. This may be due to the presence of less available active sites of AC-CF, as a result of the low surface area and less acidic functional groups.

Fig. 6(b) presents the model of intra-particle diffusion and the multi-linearity of plots. There were three steps occurring in the TMP adsorption. The initial stage of the plot indicated the diffusion of TMP through the solution to the external surface of the AC. The intra-particle diffusion occurred in the second stage, and the third stage was regarded as the final equilibrium due to extremely low TMP concentration left in solution and the reduction of interior active sites. The possible explanation is that an abundance of vacant surface active sites were available for TMP adsorption during the first stage, and then, the remaining small number of vacant surface sites were difficult to be occupied due to the extremely low TMP concentration left in solution, the reduction of interior active sites and the repulsive forces between the adsorbates on the adsorbents and bulk phase.

3.6. Adsorption isotherms

The adsorption equilibrium data were tested with the Langmuir and Freundlich equations to predict the adsorption mechanisms and assess the correlation between the amounts of adsorbates adsorbed onto ACs and adsorbate concentration in aqueous solution. Langmuir isotherm model and Freundlich isotherm model are commonly expressed as follows:

$$\frac{C_e}{q_e} = \frac{1}{q_m K_L} + \frac{1}{q_m} C_e \tag{5}$$

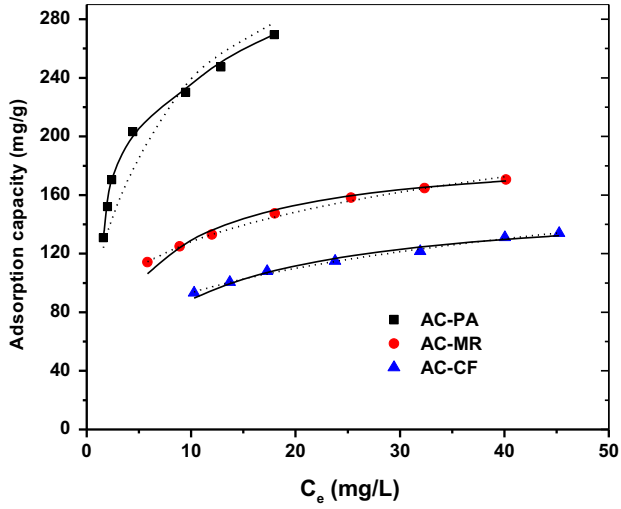

Fig. 7. Adsorption isotherms of TMP onto ACs. Solid and dashed lines represent Langmuir model and Freundlich model fitting to the data, respectively.

Table 5
Isotherm model constants for TMP adsorption onto adsorbents

Samples	Langmuir			Freundlich		
	q_m (mg/g)	K_L (L/mg)	R^2	K_F (mg^{1-n} L^n/g)	$1/n$	R^2
AC-PA	294.1	0.5074	0.9969	79.91	0.2701	0.9563
AC-MR	188.7	0.2427	0.9988	78.8	0.2123	0.9966
AC-CF	153.8	0.1354	0.9974	53.55	0.241	0.9954

$$\log q_e = \log K_F + \left(\frac{1}{n}\right) \log C_e \quad (6)$$

where q_e (mmol/g) is the amount of TMP adsorbed by ACs at equilibrium; C_e (mmol/L) is the equilibrium concentration of TMP; q_m in Eq. (5) is the maximum amount of TMP that form a complete monolayer on the adsorbents' surface; k_L in Eq. (5) is the adsorption equilibrium constant (L/mmol). k_F ($mmol^{1-1/n}$ $L^{1/n}$/g) and n in Eq. (6) is the Freundlich constant, representing the adsorption capacity of the adsorbent and adsorption intensity, respectively [30–32].

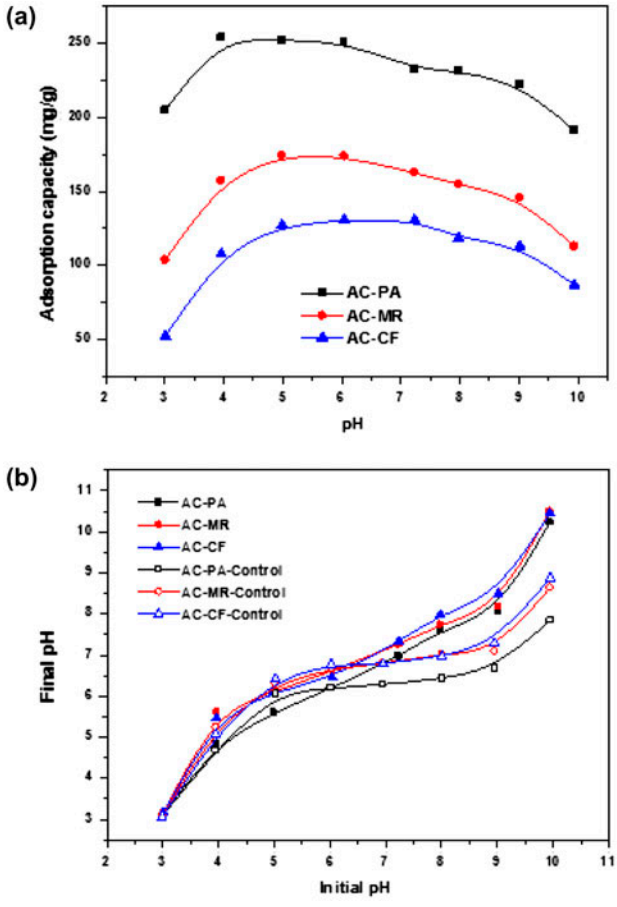

Fig. 8. Effects of pH on TMP adsorption onto AC-PA, AC-MR, and AC-CF.

The adsorption isotherms are presented in Fig. 7 and the isotherm constants are calculated and listed in Table 5. It can be observed that the adsorption data of TMP onto AC-PA were well fitted by Langmuir equation with an excellent correlation coefficients R^2 ($R^2 > 0.99$), suggesting that the adsorption occurred identical and equivalent at a fixed number of definite sites. The experimental data of TMP onto AC-MR and AC-CF could also be fitted well by both equations (Langmuir and Freundlich isotherm models), which were statistically confirmed by giving greater R^2 values ($R^2 > 0.99$). Therefore, it appears that monolayer and multilayer adsorption take place simultaneously on the surface of AC-MR and AC-CF. This indicates that both chemisorption and physisorption take place simultaneously for TMP adsorption onto the adsorbents. The values of K_L were between 0 and 1.0 (see Table 5), indicating that the adsorption of TMP onto AC-PA, AC-MR and AC-CF were favorable.

3.7. Effect of pH on TMP adsorption

Fig. 8(b) shows the equilibrium pH of the control and AC samples. Comparing the equilibrium pH of all samples under acidic conditions, it was found that the final pH of the control samples were higher than those of AC samples. This indicates that the adsorption of TMP is accompanied by releasing H^+ ions into the bulk solution. Moreover, Lewis acid–base interactions existed between amino groups of TMP and carboxylic and phenolic hydroxy groups, indicating the reaction between $-NH_3^+$ groups and the acidic groups (especially carboxylic groups) is another contributor to the lower final pH of AC samples. Lewis acid–base interactions can also be observed from the higher final pH levels for the AC samples compared with those for the control samples at high initial pH, as fewer acidic groups were left for neutralizing excess OH^- ions in the solution [33].

ACs had the same types of adsorptive interactions with TMP species in this study. However, they

Table 6
Comparison of the maximum adsorption capacities of TMP onto various adsorbents

Adsorbent	Adsorption capacities (mg/g)	Refs.
AC-PA	244.9	This work
AC-MR	165.6	This work
AC-CF	124.2	This work
AC-H_3PO_4	290.2	[20]
AC-HPO_3	81.3	
AC-H_3PO_3	58.1	
Feather charcoal	139.18	[23]
Carbon black	156.2	[34]
Montmorillonite KSF	50.0	[35]
K10	60.0	[36]

exhibited different varying trends (Fig. 8(a)), which were mainly attributed to the difference in the amounts of acidic and basic groups in the ACs. These groups can neutralize excess H^+ and OH^- ions in the bulk solution, and affect the speciation of TMP, eventually resulting in different adsorption patterns. As shown in Fig. 8(a), the TMP adsorption capacities of the ACs increase with increasing pH, and then decrease with pH. The less TMP adsorption at low pH may be attributed to the electrostatic repulsion as well as the competition from excess H^+ ions in the solution. Since TMP was dominantly in the cationic form and the ACs' surface was negatively charged at moderate initial pH levels (5–8), the enhanced electrostatic attraction would promote TMP adsorption.

Table 6 shows the comparison of the maximum adsorption capacities of TMP onto various adsorbents. Although the values reported in other studies were obtained under different experimental conditions, they may be useful as a criterion for comparing the adsorption capacities. It can be seen that the adsorption capacity of TMP in this study was relatively large.

4. Conclusions

The three biomass waste-based ACs were systematically studied in terms of their physicochemical characteristics and adsorptive properties were systematically studied. It was found that: (1) lignocellulose-based ACs exhibited more developed pore structure than keratin-based ACs; (2) lignocellulose-based ACs has more content of O and favorable acidic surface functional groups, while keratin-based ACs had more basic surface functional groups due to more content of N in its precursors; (3) $H_4P_2O_7$ activation of precursors (PA, MR, and CF) was proved to be feasible, evidenced by the produced high-quality ACs with high surface area and favorable total surface functional groups; (4) compared with AC-MR and AC-CF, AC-PA exhibited a larger adsorption capacity of TMP.

Acknowledgements

This work was supported by the Independent Innovation Foundation of Shandong University (2012JC029), Natural Science Foundation for Distinguished Young Scholars of Shandong province (JQ201216) and National Water Special Project (2012ZX07203-004).

References

[1] R.C. Bansal, M. Goyal, Activated Carbon Adsorption, CRC Press, Boca Raton, FL, 2005.
[2] B. Hameed, A. Rahman, Removal of phenol from aqueous solutions by adsorption onto activated carbon prepared from biomass material, J. Hazard. Mater. 160 (2008) 576–581.
[3] X. He, P. Ling, M. Yu, X. Wang, X. Zhang, M. Zheng, Rice husk-derived porous carbons with high capacitance by $ZnCl_2$ activation for supercapacitors, Electrochim. Acta 105 (2013) 635–641.
[4] X. He, P. Ling, J. Qiu, M. Yu, X. Zhang, C. Yu, M. Zheng, Efficient preparation of biomass-based mesoporous carbons for supercapacitors with both high energy density and high power density, J. Power Sources 240 (2013) 109–113.
[5] W.-G. Li, X.-J. Gong, K. Wang, X.-R. Zhang, W.-B. Fan, Adsorption characteristics of arsenic from micro-polluted water by an innovative coal-based mesoporous activated carbon, Bioresour. Technol. 165 (2014) 166–173.
[6] S.A. Patil, S. Chigome, C. Hägerhäll, N. Torto, L. Gorton, Electrospun carbon nanofibers from polyacrylonitrile blended with activated or graphitized carbonaceous materials for improving anodic bioelectrocatalysis, Bioresour. Technol. 132 (2013) 121–126.
[7] K. Nakagawa, S.R. Mukai, K. Tamura, H. Tamon, Mesoporous activated carbons from phenolic resins, Chem. Eng. Res. Des. 85 (2007) 1331–1337.
[8] N. Rambabu, R. Azargohar, A.K. Dalai, J. Adjaye, Evaluation and comparison of enrichment efficiency of physical/chemical activations and functionalized activated carbons derived from fluid petroleum coke for environmental applications, Fuel Process. Technol. 106 (2013) 501–510.
[9] A. Aygün, S. Yenisoy-Karakaş, I. Duman, Production of granular activated carbon from fruit stones and nutshells and evaluation of their physical, chemical and adsorption properties, Microporous Mesoporous Mater. 66 (2003) 189–195.
[10] Z. Guo, X. Bian, J. Zhang, H. Liu, C. Cheng, C. Zhang, J. Wang, Activated carbons with well-developed microporosity prepared from *Phragmites australis* by potassium silicate activation, J. Taiwan Inst. Chem. Eng. 45 (2014) 2801–2804.
[11] C. Cheng, J. Zhang, Y. Mu, J. Gao, Y. Feng, H. Liu, Z. Guo, C. Zhang, Preparation and evaluation of activated carbon with different polycondensed

phosphorus oxyacids (H_3PO_4, $H_4P_2O_7$, $H_6P_4O_{13}$ and $C_6H_{18}O_{24}P_6$) activation employing mushroom roots as precursor, J. Anal. Appl. Pyrolysis 108 (2014) 41–46.
[12] H. Liu, J. Zhang, W. Liu, N. Bao, C. Cheng, C. Zhang, Preparation and characterization of activated charcoals from a new source: Feather, Mater. Lett. 87 (2012) 17–19.
[13] L. Wang, Y. Guo, B. Zou, C. Rong, X. Ma, Y. Qu, Y. Li, Z. Wang, High surface area porous carbons prepared from hydrochars by phosphoric acid activation, Bioresour. Technol. 102 (2011) 1947–1950.
[14] J.N. Sahu, J. Acharya, B.C. Meikap, Optimization of production conditions for activated carbons from Tamarind wood by zinc chloride using response surface methodology, Bioresour. Technol. 101 (2010) 1974–1982.
[15] A. Elmouwahidi, Z. Zapata-Benabithe, F. Carrasco-Marín, C. Moreno-Castilla, Activated carbons from KOH-activation of argan (*Argania spinosa*) seed shells as supercapacitor electrodes, Bioresour. Technol. 111 (2012) 185–190.
[16] Y. Guo, D.A. Rockstraw, Physical and chemical properties of carbons synthesized from xylan, cellulose, and Kraft lignin by H_3PO_4 activation, Carbon 44 (2006) 1464–1475.
[17] M.A. Nahil, P.T. Williams, Pore characteristics of activated carbons from the phosphoric acid chemical activation of cotton stalks, Biomass Bioenergy 37 (2012) 142–149.
[18] A. Castro-Muñiz, F. Suárez-García, A. Martínez-Alonso, J. Tascón, Activated carbon fibers with a high content of surface functional groups by phosphoric acid activation of PPTA, J. Colloid Interface Sci. 361 (2011) 307–315.
[19] Y. Sun, Q. Yue, B. Gao, Y. Wang, Y. Gao, Q. Li, Preparation of highly developed mesoporous activated carbon by $H_4P_2O_7$ activation and its adsorption behavior for oxytetracycline, Powder Technol. 249 (2013) 54–62.
[20] H. Liu, J. Zhang, N. Bao, C. Cheng, L. Ren, C. Zhang, Textural properties and surface chemistry of lotus stalk-derived activated carbons prepared using different phosphorus oxyacids: Adsorption of trimethoprim, J. Hazard. Mater. 23 (2012) 5367–5375.
[21] S.H. Kim, H.K. Shon, H.H. Ngo, Adsorption characteristics of antibiotics trimethoprim on powdered and granular activated carbon, J. Ind. Eng. Chem. 16 (2010) 344–349.
[22] Y. Gao, Q. Yue, B. Gao, Y. Sun, W. Wang, Q. Li, Y. Wang, Comparisons of porous, surface chemistry and adsorption properties of carbon derived from *Enteromorpha prolifera* activated by $H_4P_2O_7$ and KOH, Chem. Eng. J. 232 (2013) 582–590.
[23] C. Cheng, J. Zhang, C. Zhang, H. Liu, W. Liu, Preparation and characterization of charcoal from feathers and its application in trimethoprim adsorption, Desalin. Water Treat. 52 (2014) 5401–5412.
[24] M. Valix, W. Cheung, G. McKay, Preparation of activated carbon using low temperature carbonisation and physical activation of high ash raw bagasse for acid dye adsorption, Chemosphere 56 (2004) 493–501.
[25] R. Usman, Y. Yokogawa, A. Mihata, J. Kurawaki, Facile synthesis of silver nanoparticles using a novel benzenethiol derivative: Addition effect of cationic surfactants, e-J. Surf. Sci. Nanotech. 13 (2015) 440–444.
[26] H. Liu, W. Ning, P. Cheng, J. Zhang, Y. Wang, C. Zhang, Evaluation of animal hairs-based activated carbon for sorption of norfloxacin and acetaminophen by comparing with cattail fiber-based activated carbon, J. Anal. Appl. Pyrolysis 101 (2013) 156–165.
[27] H. Liu, W. Liu, J. Zhang, C. Zhang, L. Ren, Y. Li, C. Cheng, Removal of cephalexin from aqueous solutions by original and Cu(II)/Fe(III) impregnated activated carbons developed from lotus stalks kinetics and equilibrium studies, J. Hazard. Mater. 185 (2011) 1528–1535.
[28] W. Weber, J. Morris, Kinetics of adsorption on carbon from solution, J. Sanit. Eng. Div. Am. Soc. Civ. Eng. 89 (1963) 31–60.
[29] C. Valderrama, X. Gamisans, F. De las Heras, J. Cortina, A. Farran, Kinetics of polycyclic aromatic hydrocarbons removal using hyper-cross-linked polymeric sorbents Macronet Hypersol MN200, React. Funct. Polym. 67 (2007) 1515–1529.
[30] M.A. Hossain, H.H. Ngo, W.S. Guo, L.D. Nghiem, F.I. Hai, S. Vigneswaran, T.V. Nguyen, Competitive adsorption of metals on cabbage waste from multi-metal solutions, Bioresour. Technol. 160 (2014) 79–88.
[31] I. Langmuir, The adsorption of gases on plane surfaces of glass, mica and platinum, J. Am. Chem. Soc. 40 (1918) 1361–1403.
[32] H. Freundlich, Over the adsorption in solution, J. Phys. Chem. 57 (1906) 385–470.
[33] H. Liu, J. Zhang, H.H. Ngo, W.S. Guo, H.M. Wu, Z.Z. Guo, C. Cheng, C.L. Zhang, Effect on physical and chemical characteristics of activated carbon on adsorption of trimethoprim: Mechanisms study, RSC Adv. 5 (2015) 85187–85195.
[34] J.R. Dominguez-Vargas, V. Carrillo-Perez, T. Gonzalez-Montero, E.M. Cuerda-Correa, Removal of trimethoprim by a low-cost adsorbent: Influence of operation conditions, Water Air Soil Pollut. 223 (2012) 4577–4588.
[35] Z. Bekci, Y. Seki, M.K. Yurdakoc, Equilibrium studies for trimethoprim adsorption on montmorillonite KSF, J. Hazard. Mater. 133 (2006) 233–242.
[36] Z. Bekçi, Y. Seki, M.K. Yurdakoc, A study of equilibrium and FTIR, SEM/EDS analysis of trimethoprim adsorption onto K10, J. Mol. Struct. 827 (2007) 67–74.